energies

Article

Cost-Effective Optimization of an Array of Wave Energy Converters in Front of a Vertical Seawall

Senthil Kumar Natarajan and Il Hyoung Cho *

Department of Ocean System Engineering, Jeju National University, Jeju 690-756, Republic of Korea; senthil@stu.jejunu.ac.kr
* Correspondence: cho0904@jejunu.ac.kr; Tel.: +82-64-754-3482; Fax: +82-64-751-3480

Abstract: The present paper focuses on investigating the cost-effective configuration of an array of wave energy converters (WECs) composed of vertical cylinders situated in front of a vertical seawall in irregular waves. First, the hydrodynamic calculations are performed using a WAMIT commercial code based on linear potential theory, where the influence of the vertical wall is incorporated using the method of image. The viscous damping experienced by the oscillating cylinder is considered through CFD simulations of a free decay test. A variety of parameters, including WEC diameter, number of WECs, and the spacing between them, are considered to determine an economically efficient WEC configuration. The design of the WEC configuration is aided by a cost indicator, defined as the ratio of the total submerged volume of the WEC to overall power capture. The cost-effective configuration of WECs is achieved when WECs are positioned in front of a vertical wall and the distance between them is kept short. It can be explained that the trapped waves formed between adjacent WECs as well as the standing waves in front of a seawall significantly intensify wave fields around WECs and consequently amplify the heave motion of each WEC. A cost-effective design strategy of WEC deployment enhances the wave energy greatly and, consequently, contributes to constructing the wave energy farm.

Keywords: wave energy converter; cost-effective analysis; method of image; linear potential theory; vertical seawall

check for updates

Citation: Natarajan, S.K.; Cho, I.H. Cost-Effective Optimization of an Array of Wave Energy Converters in Front of a Vertical Seawall. *Energies* **2024**, *17*, 128. https://doi.org/10.3390/en17010128

Academic Editors: Konstantinos Aravossis and Eleni Strantzali

Received: 30 November 2023
Revised: 19 December 2023
Accepted: 22 December 2023
Published: 25 December 2023

1. Introduction

The urgency to address global warming and the resulting climate changes highlights the necessity of reducing greenhouse gas emissions, particularly within the energy sector, where electricity and heat production are the largest contributors to global emissions [1]. Meanwhile, energy demand continues to surge. As a promising solution for curbing greenhouse gas emissions, renewable energy, notably solar and wind power, is projected to contribute 43% of the world's electricity by 2030, a significant increase from the current level of 28% [2]. Notably, wave energy boasts a higher power density compared to solar and wind energy. For instance, at a latitude of 15° N within the Northeast Trades, the average power density is 0.17 kW/m^2 for solar, 0.58 kW/m^2 for wind, and 8.42 kW/m^2 for wave energy [3]. Despite its higher potential, wave energy has not yet achieved commercial viability similar to solar and wind power sources due to its levelized cost of energy still lacking competitiveness with other renewable sources [4]. Wave energy exhibits greater availability compared to solar and wind energy, as it remains available both day and night, and persists throughout the entire year. Hence, achieving cost-effectiveness in harnessing wave energy is essential for establishing it as a financially feasible choice among renewable energy alternatives.

There have been many studies focusing on optimizing wave energy converters (WECs) for maximizing power extraction so that they become economically viable. In [5], an optimization of dimensions and layout of an array of heaving buoy WECs have been carried out. A control method is proposed in [6] for an array of WECs maximizing power and satisfying constraints for optimal energy extraction performance, with full consideration of wave and multi-body interactions, as multiple WECs instead of stand-alone devices could increase energy production by over 15% per device. In [7], a comprehensive assessment is carried out focusing on the geometric optimization of wave energy conversion devices. This review offers a critical analysis of the current state-of-the-art in geometry optimization and outlines its limitations. Similarly, [8] provides a review of the geometry optimization of WECs, aiming to discover enhanced hull shapes that can maximize power generation while minimizing the associated costs. An investigation into the hydrodynamic optimization of a sloped motion point absorber WEC has been conducted in [9] using a time-efficient frequency-domain numerical model. In [10], the authors presented a size optimization of WECs on a floating wind–wave combined power generation platform, which has a significant increase in power generation compared with the single point absorber. The structural optimization of oscillating-array buoys was performed in [11] to improve the wave energy capture efficiency with the simulated models of different spacing, placement modes, and actuating arm lengths of buoys. A review was conducted and presented in [12] for the optimal configuration of wave energy conversions concerning nearshore wave energy potential where WECs' shape optimization may significantly boost performance, and where if it is combined with the PTO control approach may lead to better outcomes. In [13], power take-off optimization has been carried out to maximize energy conversion with a two-body WEC system utilizing relative heave motion to extract power.

One method to increase wave power absorption is by positioning WECs in front of a reflective structure which can amplify the WEC's motion, thereby extracting higher power. The authors of [14] analyzed the hydrodynamic performance of a series of truncated cylinders positioned in front of a vertical wall in the frequency domain. This examination aimed to explore the impact of wave reflections coupled with disturbances caused by the bodies themselves. An experimental evaluation was conducted in [15] to determine the hydrodynamic performance of a WEC system integrated into a breakwater, in comparison with conventional WECs. The WECs positioned in front of the breakwater experience increased heave motion, indicating that the presence of the breakwater enhances the energy conversion performance of the WEC array. In [16], the authors conducted a hydrodynamic investigation into an innovative breakwater featuring parabolic openings designed to harness wave energy. Truncated cylinder-type WECs were positioned in front of these openings, which effectively converge propagating waves toward a focal point. This configuration notably increased the extracted wave power. A theoretical assessment of the hydrodynamic attributes of arrays consisting of vertical axisymmetric floaters of various shapes positioned in front of a vertical breakwater was conducted [17] using an analytical method. The image method was utilized to simulate the breakwater's influence on the array. The study investigated three distinct types of floaters and various array configurations situated in front of the vertical wall. The hydrodynamic coefficients either increased or decreased depending on the distance between the wall and the floater. The investigation delved further in [18] into evaluating an array of cylindrical WECs with a vertical symmetry axis positioned in front of a reflective vertical breakwater. This study explored three distinct array configurations: parallel, perpendicular, and rectangular arrangements, considering various distances from the wall, inter-body spacing, wave heading angles, and mooring stiffness values. Results indicated that the most power-efficient WEC arrangement was the one aligned parallel to the breakwater. Additionally, the deployment of WECs in closer proximity to the breakwater demonstrated higher power efficiency across the majority of wave frequencies compared to WECs positioned farther away. Moreover, the presence of the breakwater positively influenced the system's power absorption, significantly enhancing absorbed power across various arrangements, wave angles, and inter-body spacings. This amplification effect was particularly notable for the parallel, close-to-wall configuration across incoming wave angles. In [19], the hydrodynamic efficiency of a WEC placed in front of a bottom-seated, surface-piercing, vertical orthogonal breakwater in the frequency domain has been analyzed. A theoretical approach, employing the image method, was utilized to simulate how the walls affected the device's power absorption, taking into account the infinite length of the walls' arms. The wave power absorption of WEC five by five arrays and a single array of five WECs positioned in front of a vertical wall were computed in [20,21] using an in-house transient wave-multi-body numerical tool called ITU-WAVE, respectively. This tool employed a marching scheme to solve boundary integral equations for analyzing hydrodynamic radiation and exciting forces. The method of images accounted for the perfect reflection of incident waves from the vertical wall. Numerical findings revealed significantly enhanced performance and wave power absorption of WEC arrays in front of a vertical wall compared to arrays without this vertical wall effect. This heightened efficiency primarily resulted from the presence of standing and nearly trapped waves between the vertical wall and the WEC arrays, along with robust interactions between the WECs themselves.

The present models used for estimating the expenses associated with a wave energy project are often oversimplified, leading to a wide range of economic assessments. This variability in evaluations raises uncertainties for potential investors, thus hindering the progress of wave energy development. Indeed, comprehending the costs associated with wave energy is a pivotal area of research within marine renewable energy. Within this context, the paper [4] provides a comprehensive review of all factors essential for an economic analysis of wave energy. This includes considering numerous elements that are typically overlooked. The study aimed to delineate both direct and indirect costs of a wave farm, encompassing preliminary expenses, construction, operational, and maintenance costs, as well as decommissioning costs, alongside potential revenues. The expense associated with WECs constitutes a substantial portion of the total cost of a wave farm. Similar to other renewable sources like solar photovoltaic (PV) and solar thermal systems, the current capital costs for wave energy surpass those of conventional generation technologies such as gas and coal. Nonetheless, these expenses are anticipated to decline as economies of scale come into play with increased wave farm installations. This trend, coupled with the uncertainty surrounding long-term fuel costs and rising construction expenses for traditional generation technologies, is leading to a narrowing of the significant gaps in electricity costs that were previously evident. Additionally, the operational and maintenance costs are notably high, given the sea environment. Concerning the revenues generated by a wave farm, the primary source of income naturally stems from the sale of the generated energy. Currently, WECs exhibit relatively low performance levels, and enhancing their efficiency will significantly strengthen the economic feasibility of wave energy.

In [22], a comprehensive techno-economic optimization of a floating WEC was conducted using a genetic algorithm considering a wide multi-variate design space. This included considerations of the floater's shape, dimensions, subcomponent configuration, and characteristics. Similarly, a techno-economic assessment of the influence on the sizing of WECs was conducted [23]. The articles [24,25] provided economic evaluations and cost estimations for WECs during their initial developmental phases. To assess the cost-effectiveness of WECs in power generation, Ref. [26] introduces a cost indicator that mirrors the expenses linked to WECs, as they constitute a significant portion of the overall project cost.

Although there have been research works on parametric analysis of configurations of WECs in regular waves, exploring the application of prototype-scale WECs in an array subjected to irregular waves is crucial. Specifically, varying key parameters like WEC diameters, the number of WECs, and their spacing while situating them in front of a vertical seawall would provide valuable insights into the hydrodynamic interaction among the WECs themselves and with the reflective wall at the sea site. Therefore, finding an efficient configuration coupled with effective PTO damping is essential for optimization to maximize power extraction, which should also factor into the economic aspect to make it a commercially viable option. Hence, the objective of this research is to conduct an analysis aimed at identifying a cost-efficient arrangement for an array of point absorber-type WECs installed in front of a vertical seawall in irregular waves. Vertical cylindrical floaters have been selected as the WECs, with varying parameters like diameter, number of WECs, and spacing between them, to determine an economically efficient configuration for harnessing wave energy. To facilitate this process, a cost indicator [26] is utilized, representing the ratio of submerged volume to power capture, which provides insight into the cost associated with extracting a unit of electrical power. The hydrodynamic calculations have been performed using the linear potential theory, and the method of image [17–21] has been employed to account for the influence of the vertical wall. The viscous damping was obtained from a computational fluid dynamics (CFD) simulation of heave-free decay test. Optimal PTO damping at the natural frequency as well as PTO damping that results in maximum power output under irregular waves are considered to maximize power extraction.

2. Methodology

An array of N vertical cylindrical WECs is placed in front of a vertical seawall, which is perfectly reflective throughout the constant water depth h. The diameter and draft of WECs are D and d, respectively. WECs are placed at a distance L_w from a seawall in a parallel arrangement, whereas the distance between WECs is L. WECs are independently oscillating vertically in waves while the other modes of motion are restricted. An array of WECs is exposed to plane incident waves with angular frequency ω and amplitude A propagating into the negative x-axis. Figure 1 depicts the array of WECs placed in front of a vertical seawall.

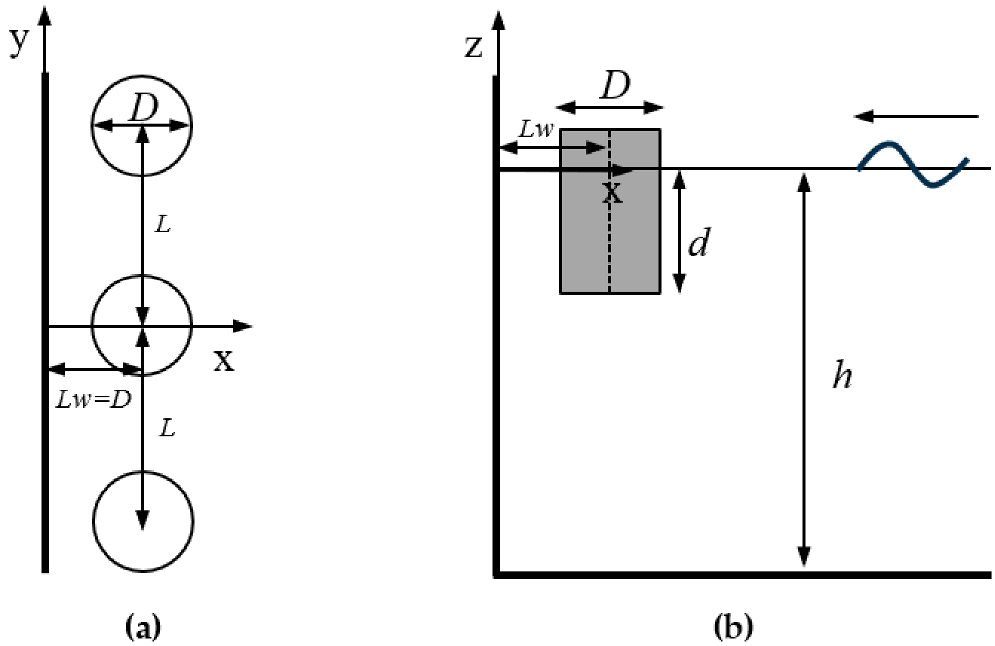

Figure 1. Definition sketch of an array of vertical cylindrical WECs placed in front of a vertical seawall. (**a**) top view (**b**) side view.

2.1. Hydrodynamic Model

The added mass, radiation damping, and wave excitation force on the WECs are computed numerically from a panel-based commercial software WAMIT (Version 7.1), which is widely used in computing wave loads and motions of offshore structures and floating vessels. The linear potential theory has been used in numerical modeling under the assumption of small amplitude, inviscid and incompressible fluid, and irrotational flow. When a floating body oscillates near a rigid lateral boundary like a vertical seawall, the interaction between them must be accounted for. Conventionally, the effect of a rigid wall can be considered by imposing the no-flux boundary condition $\frac{\partial \phi}{\partial n} = 0$ on a rigid wall. However, a more convenient approach is to replace the effect of a seawall with an image body, which is placed symmetrically on the opposite side of the wall, with a prescribed motion to ensure that the boundary condition on the seawall is satisfied [17–21]. Figure 2 shows a top view of an array of WECs positioned in front of a vertical seawall, which is replaced with image bodies.

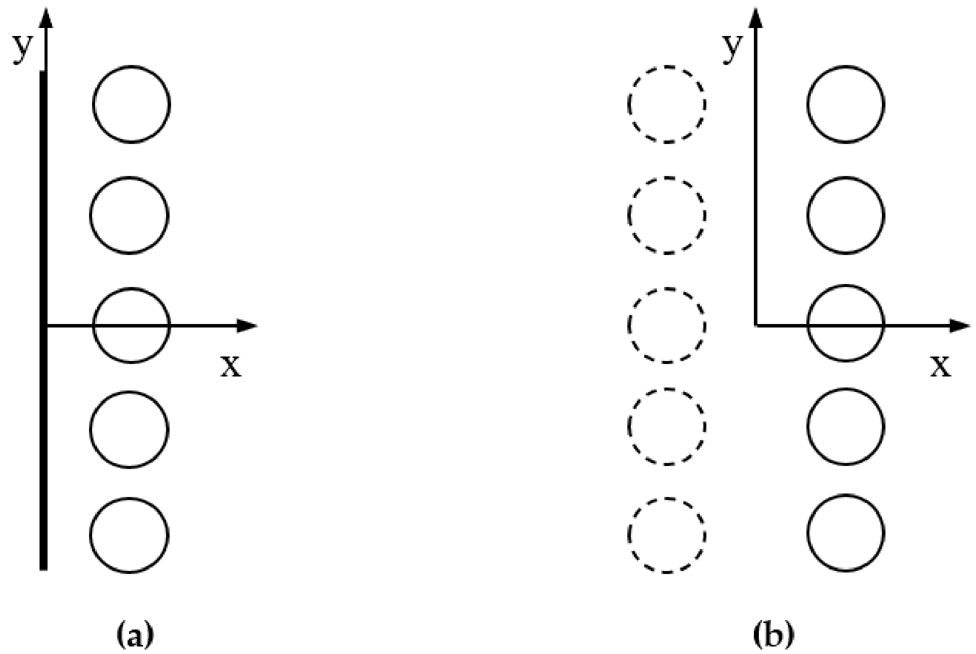

Figure 2. Top view of an array of (**a**) WECs in front of a vertical seawall and (**b**) WECs and image bodies denoted by a dashed line to replace the vertical seawall.

In this approach, let us consider the WEC p placed in front of the vertical seawall, which is replaced with an image WEC p' symmetrically placed on the opposite side of the seawall. The hydrodynamic parameters of the WEC p with the influence of the vertical seawall can be obtained by combining the hydrodynamic parameters of the forced oscillation of the WEC p and its image p' effect, in the respective mode of motion. For instance, the surge added mass, radiation damping coefficient, and wave excitation force can be derived [17] as $a_{11}^{p} - a_{11}^{p'}$, $b_{11}^{p} - b_{11}^{p'}$ and $f_1^{p} - f_1^{p'}$ respectively. Similarly, the heave added mass, radiation damping coefficient, and wave excitation force can be obtained by $a_{33}^{p} + a_{33}^{p'}$, $b_{33}^{p} + b_{33}^{p'}$, and $f_3^{p} + f_3^{p'}$, respectively. a_{ij}^{p}, b_{ij}^{p} and f_i^{p} are the hydrodynamic forces of the p floater in i-th direction due to j-th mode of motion, where 1 and 3 denote the surge motion and heave motion respectively.

2.2. Equation of Motion

The p-th WEC is independently oscillating with a vertical mode in incident waves, with the other modes of motion being constrained. The wave power has been extracted with a power take-off (PTO) system, which converts the heave motion of the WEC into electricity. The PTO system is realized by an equivalent linear damping force. The schematic diagram of the WEC in heave motion is shown in Figure 3.

The equation of heave motion can be written as [27–30]

$$(m^p + a_{33}^{p})\ddot{z}_p + (b_{33}^{p} + b_{vis}^{p} + b_{PTO}^{p})\dot{z}_p + c_{33}^{p} z_p = f_3^{p} \quad (1)$$

where m^p is a mass of the p-th WEC, a_{33}^{p}, b_{33}^{p}, f_3^{p} are the frequency-dependent heave added mass, radiation damping coefficient, and wave excitation force respectively, c_{33}^{p} is the heave restoring force coefficient, and b_{vis}^{p} is the heave viscous damping coefficient, which is obtained by

$$b_{vis}^{p} = \frac{2\kappa^{p} c_{33}^{p}}{\omega_{N}^{p}} - b_{33}^{p}(\omega_{N}^{p}) \tag{2}$$

where the undamped heave natural frequency is given by $\omega_N^p = \sqrt{\frac{c_{33}^p}{m^p + a_{33}^p(\omega_N^p)}}$. The damping factor κ^p for the heave mode can be obtained from the heave-free decay test, which can be conducted experimentally or using a CFD simulation. In the present study, the heave-free decay test was conducted in a CFD simulation to obtain the viscous damping coefficient. b_{PTO}^p is the PTO damping coefficient and z_p is the heave motion response of the p-th WEC.

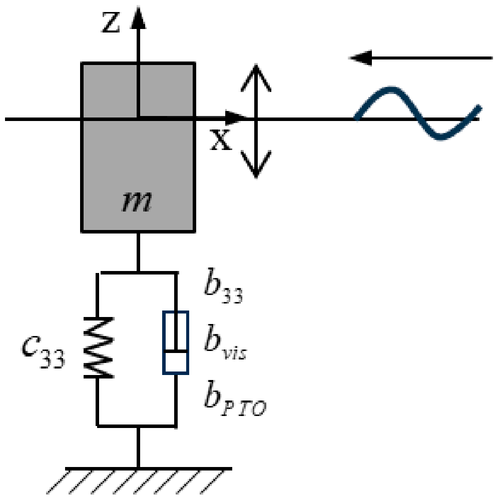

Figure 3. Schematic representation of the WEC in heave motion.

2.3. Extracted Wave Power

Wave power extracted by the WEC depends on the PTO damping and velocity of the WEC. In regular waves, the time-averaged extracted power of p-th WEC per unit wave amplitude is expressed as [27–30]

$$\overline{P}^{p}(\omega) = \frac{1}{2} b_{PTO}^{p} \omega^{2} |z_{p}|^{2} \tag{3}$$

We can extend the extracted power in regular waves to irregular waves characterized by a significant wave height $H_{1/3}$ and peak period T_P. The JONSWAP spectrum is used for the incident wave spectrum $S_\varsigma(\omega)$, which is obtained by [31]

$$\begin{aligned} S_{\varsigma}(\omega) &= \beta \frac{H_{1/3}^{2}\omega_{P}^{4}}{\omega^{5}} \exp\left[-1.25\left(\frac{\omega}{\omega_{P}}\right)^{-4}\right] \gamma^{\exp\left[-\frac{(\omega-\omega_{P})^{2}}{2\sigma^{2}\omega_{P}^{2}}\right]} \\ \text{with } \beta &= \frac{0.0624}{0.23 + 0.0336\gamma - 0.185(1.9+\gamma)^{-1}}(1.094 - 0.01915 \ln \gamma) \end{aligned} \tag{4}$$

where $\omega_P (= \frac{2\pi}{T_P})$ is the peak frequency. The peakedness factor $\gamma = 3.3$, $\sigma = 0.07$ for $\omega < \omega_P$, and $\sigma = 0.09$ for $\omega \geq \omega_P$.

The mean extracted power of the p-th WEC under the irregular waves can be obtained by [27,28,30,32,33]

$$\overline{P}_{irr}^{p} = \int_{0}^{\infty} S_{\varsigma}(\omega) \overline{P}^{p}(\omega) d\omega \tag{5}$$

Thus, the total power of N WECs in an array can be written as

$$P_{Total} = \sum_{p=1}^{N} \overline{P}_{irr}^{p} \tag{6}$$

2.4. PTO Damping

Based on Equation (3), the extracted power will be maximum under the condition of

$$\frac{d\overline{P}^{P}}{db_{PTO}^{p}} = 0 \tag{7}$$

which leads to a derivation of the frequency-dependent optimal condition of

$$\widetilde{b}_{PTO}^{p}(\omega) = \sqrt{(b_{33}^{p})^{2} + \left(\frac{c_{33}^{p}}{\omega} - \omega(m^{p} + a_{33}^{p})\right)^{2}} \tag{8}$$

Although applying the variable optimal damping coefficient $\widetilde{b}_{PTO}^{p}$ as a function of wave frequency might yield higher power extraction theoretically, it might not be practical to apply variable PTO damping in the real sea according to incoming wave frequency. Thus, adopting a single best PTO damping is desirable.

Conventionally, the optimal PTO damping at a natural frequency would be the best option as the optimal PTO damping will be $b_{PTO}^{p} = b_{33}^{p}$ at a natural frequency based on Equation (8), which will lead to a maximum power extraction at resonance. Hence the optimal PTO damping at a natural frequency can be a candidate in the maximizing of power extraction.

An alternative approach is to explore a range of PTO damping values, calculate the associated extracted power ($\overline{P}_{irr}^{p}$) for each PTO damping under the irregular waves, and then select the PTO damping that yields the maximum extracted power. In this method, as the PTO damping increases, the heave motion decreases, and these reductions are reflected as the extracted power. However, the extracted power reaches a maximum with the increase in PTO damping, after which it starts to decrease despite further increases in PTO damping. Therefore, the PTO damping that results in maximum power can be chosen as another candidate.

So, in the present study, both the optimal PTO damping at a natural frequency and the PTO damping which yields maximum power extraction are considered and compared to each other.

2.5. Cost Indicator

The cost-effectiveness configuration design of WECs is achieved by reducing the cost of energy production while increasing wave power capture. To demonstrate the cost-effectiveness design, a cost indicator [26], which is defined as a ratio of submerged volume to power capture, is being used. In an array of WECs, it is defined as a ratio of total submerged volume to the total power capture of all the WECs.

$$\text{Cost indicator} = \frac{\text{Total submerged volume } \left(\text{m}^{3}\right)}{\text{Total power capture (kW)}} \tag{9}$$

The submerged volume is used to reflect the cost of materials for energy production. Hence the large cost indicator denotes higher fabrication cost of WECs in producing unit power of electricity, which is not desirable in achieving cost-effectiveness. Thus, the analysis for a cost-effective array of WECs focuses on identifying an array of WECs with a smaller cost indicator. Hence, the ranking of cost-effective configurations has been determined based on a scale of lower to higher value of the cost indicator.

3. Numerical Results and Discussion

3.1. Validation

3.1.1. Validation of Hydrodynamic Parameters

The present numerical results of hydrodynamic forces obtained from the commercial software WAMIT are compared with the published analytical results [17] for validation purposes. The WAMIT software supplies frequency-domain solutions based on the low-order panel method for the radiation and diffraction problems under linear potential theory. The hydrodynamic parameters obtained from the WAMIT were modified using the image method to consider the vertical seawall effect.

As a numerical model, an array of five cylindrical WECs is placed in front of a vertical seawall similar to the arrangement shown in Figure 2. The diameter (D) and draft (d) of WECs are 2 m and 1 m. The water depth (h) is identical to the WEC's diameter. The distance (L) between WECs and the distance (L_w) between WECs and a vertical seawall are 8 m and 4 m, respectively. The comparison is shown with the dimensionless added mass $a_{ii}/\frac{\rho D^3}{8}$, radiation damping $b_{ii}/\frac{\omega\rho D^3}{8}$, and wave excitation force $f_i/\frac{\rho g D^2 A}{4}$ where $i = 1, 3$ denote the surge and heave motion mode, which are plotted against $kD/2$ where k is the wave number. Numerical simulations are performed for the cases without the vertical seawall and with the vertical seawall, which is based on the image method. The numerical results of the first WEC in an array denoted as WEC ① are presented here. Figures 4 and 5 show the comparison between the present numerical solutions and analytical results [17] for surge and heave hydrodynamic forces of the WEC ①. The numerical results are in perfect agreement with the analytical results.

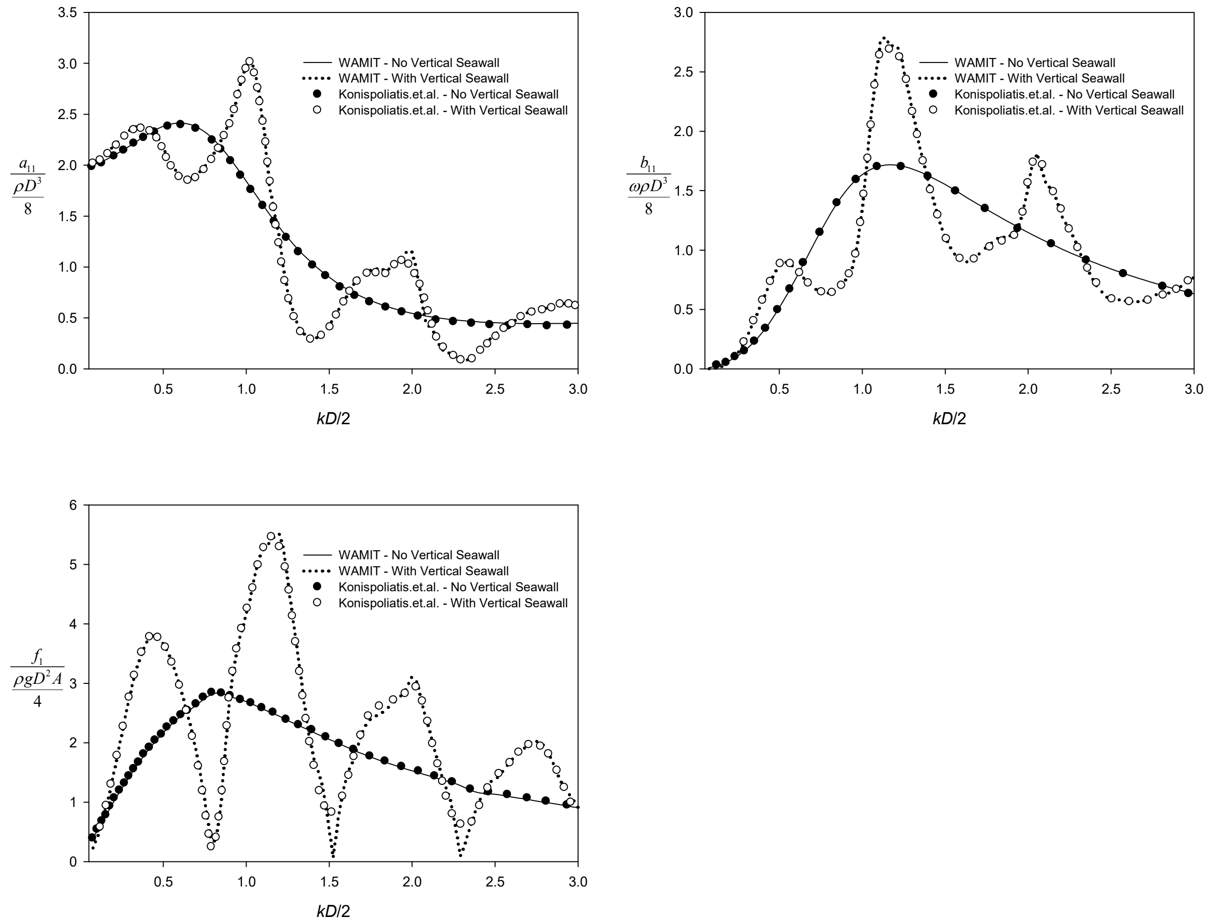

Figure 4. Dimensionless added mass, radiation damping, and wave excitation force of the WEC ① in surge mode [17].

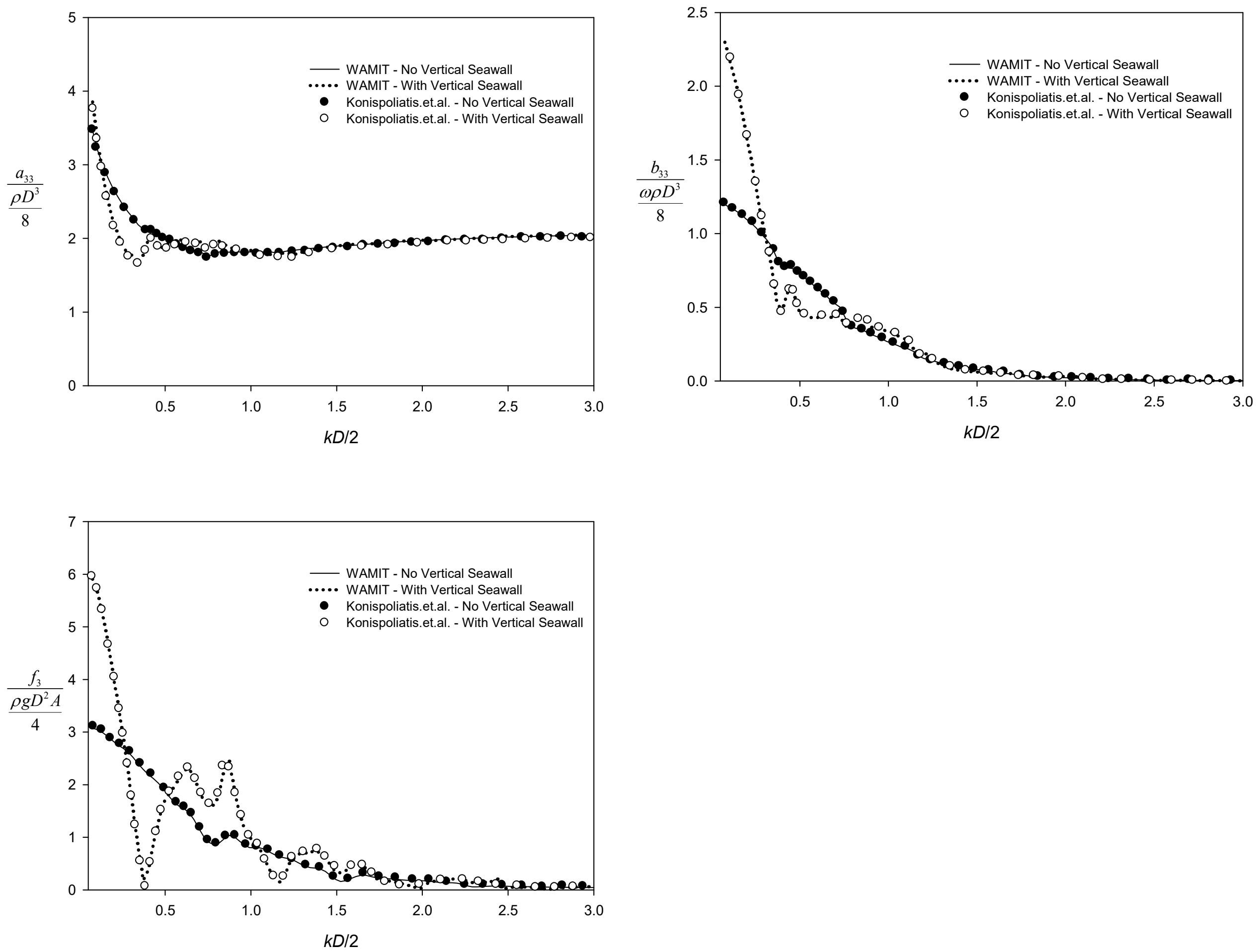

Figure 5. Dimensionless added mass, radiation damping, and wave excitation force of the WEC ① in heave mode [17].

3.1.2. Validation of CFD Simulation

The viscous damping is obtained from a CFD simulation of the free decay test in the heave direction, where the numerical calculation is performed by the commercial CFD code STAR-CCM+. The computational problem is solved by using the three-dimensional continuity, momentum, and K-Omega turbulence model with multiphase interaction in implicit unsteady time-steps. The volume of fluid (VOF) method was adopted to track the free surface in two phases (air and water). Two regions were created, one being the background region and the other surrounding WEC as an overset region with information exchanged through overlapping cells. The domain has been discretized into small cells with a trimmed cell mesher while the surface remesher was selected to create mesh around the WEC and prism layer for handling boundary layer while the domain has been created predominantly with hexahedral elements. The domain's length has been adequately extended to avoid wave reflection, with the outermost and bottom boundaries designated as walls, while the top boundary was a pressure outlet. With the finer time-step, a simulation time of four times the natural period of the WEC has been used to capture peaks of heave decay.

The computational result of the free decay test was compared with an experimental result to validate the numerical model. The model used in the experiment was a vertical cylinder with a diameter of 0.12 m and a draft of 0.25 m, which was placed in a water depth of 0.6 m. The experiment was carried out in a two-dimensional wave flume, located at Jeju National University, which was 20 m long and 0.8 m wide. The model was placed in the middle of a tank with the help of four slack mooring lines which had negligible effect on motion response. The model was initially given a displacement in the heave direction and allowed to oscillate freely. The heave motion was then tracked using image markers on the model, and Python code was used to process the video clips and extract time series data. Figure 6 shows the comparison of the numerical simulation with the experimental observation, which showed good agreement. The validated numerical model was used to simulate the free decay test of WECs with the present study to obtain the viscous damping coefficient of WECs.

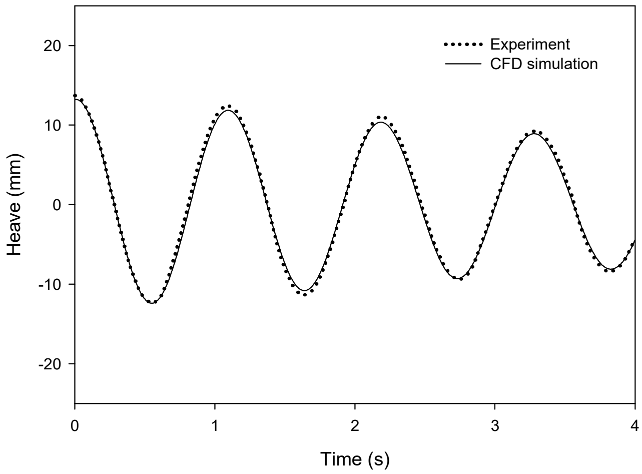

Figure 6. Comparison of experimental results with CFD simulation in the heave free decay test.

3.2. Modeling Parameters

In the calculation, the prototype WECs were considered in irregular wave climates described by a JONSWAP spectrum with a significant wave height ($H_{1/3}$) of 3 m and peak period (T_P) of 5 s. To search for a cost-effective design of WECs, various parameters of WECs such as diameter, number of WECs, and distance between them were considered. The diameters (D) considered were 2 m, 3 m, and 4 m while the drafts (d) of WECs were selected as 5.55 m, 5.25 m, and 5 m, accordingly and mass (m) of 17,872 kg, 38,038 kg and 64,403 kg respectively. These drafts were chosen to tune the heave natural period of WEC to align with the peak period of the wave spectrum such that the heave motion will be maximized at the peak frequency where wave energy is concentrated. The number of WECs under consideration were 1, 3, and 5, which enabled comparison of the performance of a single WEC and multiple WECs in an array. The distance between the WEC and the vertical seawall (L_w) is fixed to be equal to the WEC's diameter (D). The WECs are deployed with a parallel layout to the seawall. The distance between WECs (L) is considered as two- and five-times the diameter of the WEC. These can be representative values of the minimum required distance and a sufficiently distant placement respectively [18,21]. The WECs were placed in a water depth of 10 m. Figure 7 shows a schematic sketch of different configurations of an array of WECs and key parameters with a total of 15 cases.

All these design scenarios were initially tested without a vertical seawall. Subsequently, the WECs were placed in front of a vertical seawall, allowing for a comparison of how the seawall influences the performance of the WEC. Likewise, the comparison of the performance of the different sizes, the number of WECs in an array, and the distance between WECs were analyzed. As explained in Section 2.4, the extracted power was calculated for different conditions like the optimal PTO damping at a natural frequency and the PTO damping that yields maximum power extraction. Both the results were compared and analyzed.

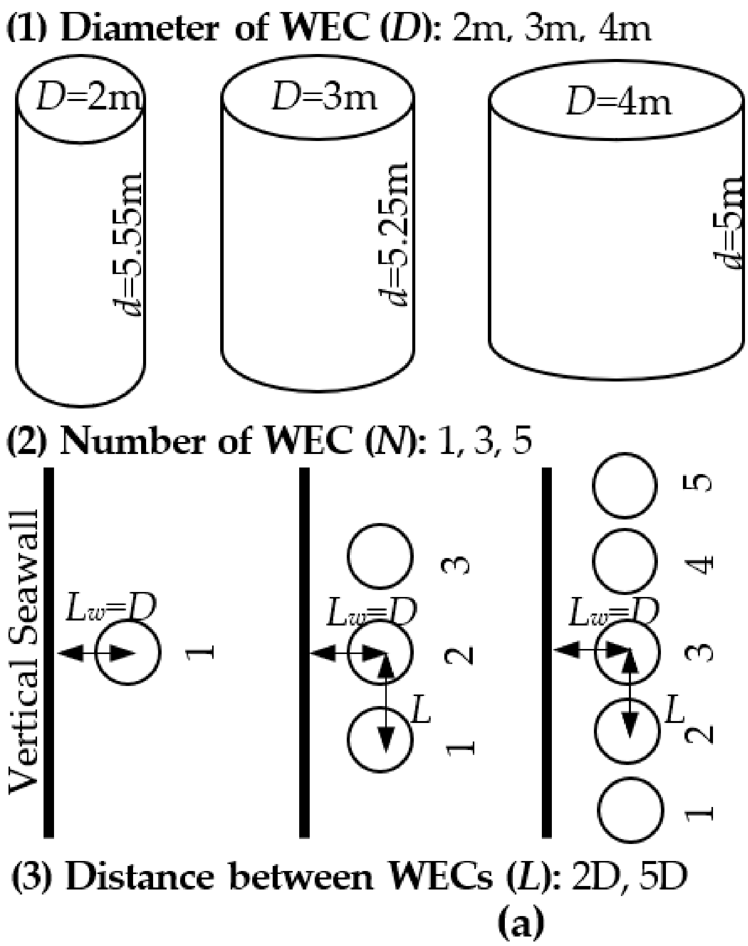

Number of WEC (N)	Distance between WEC (L)	Diameter of WEC (D)		
		2 m	**3 m**	**4 m**
1	-	Case 1	Case 6	Case 11
3	2D	Case 2	Case 7	Case 12
	5D	Case 3	Case 8	Case 13
5	2D	Case 4	Case 9	Case 14
	5D	Case 5	Case 10	Case 15

(**b**)

Figure 7. (**a**) Schematic sketch of different configurations of an array of WECs with various parameters such as WEC diameter, number of WECs, and spacing between WECs. (**b**) Various parameters in a tabular form with a total of 15 cases.

3.3. Viscous Damping

Figure 8 shows the CFD simulation of the heave-free decay test for different diameters of the WEC. The damping factor κ and damped natural period T_N are indicated inside each plot. The viscous damping coefficient b_{vis} can be obtained using Equation (2), which is proportional to the damping factor. It can be observed from the plots that as the WEC's diameter increased, the viscous damping increased due to the increase of the circumference length of the bottom of a cylinder where the generation of vortices occurs.

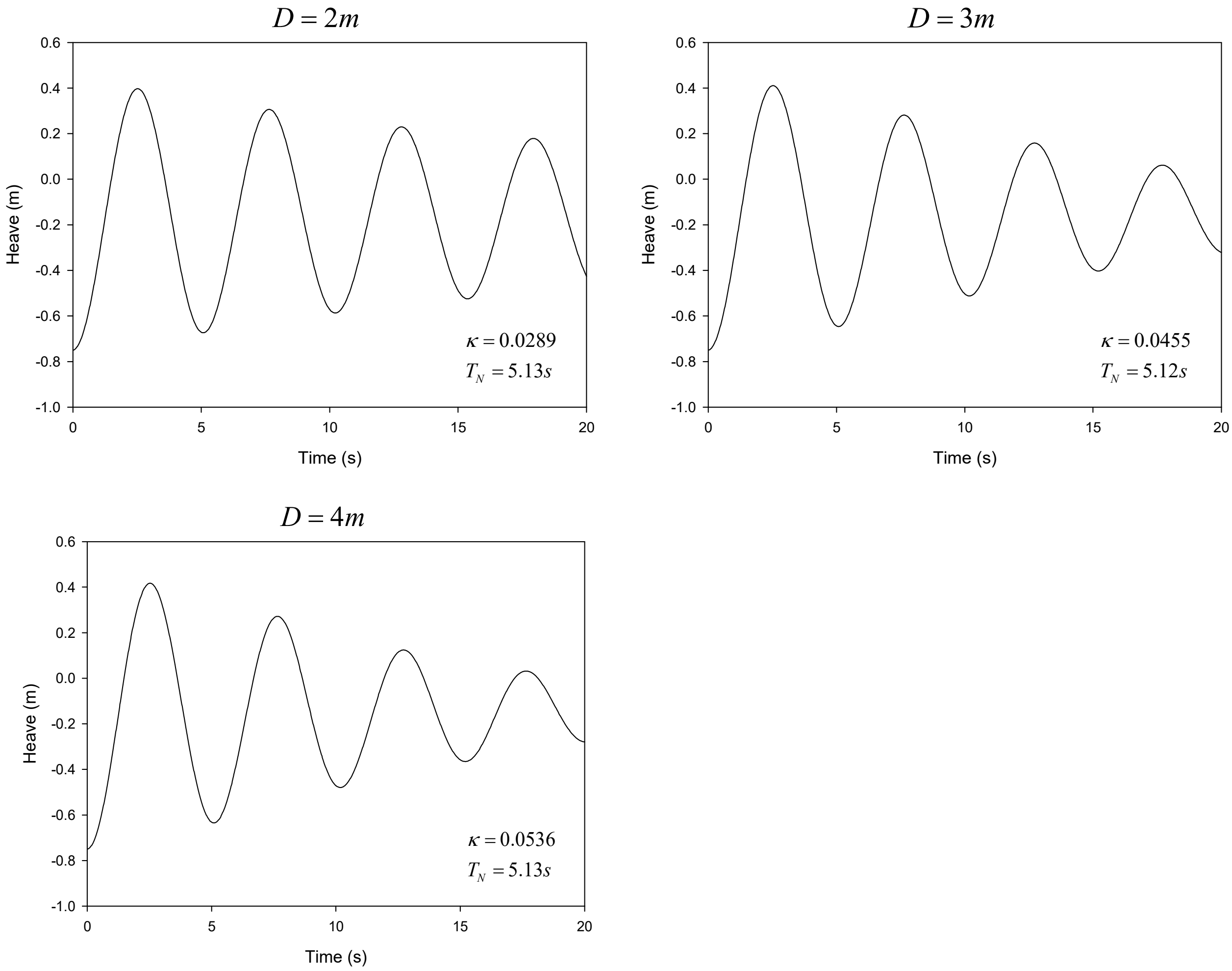

Figure 8. CFD simulation of the heave free decay test with different diameters of the WEC.

3.4. Extracted Power and Cost Indicator

The hydrodynamic parameters, computed from WAMIT with the method of image to incorporate the influence of vertical seawall, were combined with the viscous damping from CFD simulation and PTO damping. These combined parameters were then utilized to compute the heave motion of the WEC, as well as the extracted power from the PTO system and the related cost indicator under irregular wave conditions across different scenarios. A MATLAB code was used to integrate the parameters obtained from WAMIT and CFD calculations, for calculating the heave response of the WEC, along with the extracted power and cost indicators across various scenarios under irregular waves.

Table 1 provides a breakdown of the extracted power of each WEC and the total power of an array, along with the associated PTO damping and cost indicator for WECs positioned without a vertical seawall. The calculations are presented for both the optimal PTO damping at a natural frequency and the PTO damping yielding maximum power. Hereafter, these will be referred to as "optimum" and "maximum", respectively. Meanwhile, Table 2 presents corresponding data for WECs positioned in front of a vertical seawall. It can be observed that the extracted power was significantly higher with the "maximum" than the "optimum". This difference can be attributed to the higher PTO damping associated with the "maximum" resulting in increased power extraction. Likewise, the cost indicator was notably reduced with the "maximum", coinciding with the objective of cost-effectiveness.

Table 1. Extracted power and cost indicator of WECs placed in the open sea, calculated for the optimal PTO damping at a natural frequency and the PTO damping for the maxi mum power (denoted as "optimum" and "maximum" respectively).

D (m)	*N*	*L*	Case		$\overline{P}_{irr}$ (kW)		b_{PTO} (kNs/m)		P_{Total} (kW)		Cost Indicator (m^3/kW)	
					Opt	**Max**	**Opt**	**Max**	**Opt**	**Max**	**Opt**	**Max**
2	1	-	1	WEC1	1.01	3.40	0.23	3.00	1.01	3.40	17.23	5.13
	3	2D	2	WEC1	1.01	3.41	0.23	3.00	2.96	10.15	17.66	5.15
				WEC2	0.95	3.32	0.22	3.00				
				WEC3	1.01	3.41	0.23	3.00				
		5D	3	WEC1	1.05	3.50	0.24	3.00	3.18	10.55	16.46	4.96
				WEC2	1.08	3.55	0.24	3.00				
				WEC3	1.05	3.50	0.24	3.00				
	5	2D	4	WEC1	1.06	3.56	0.23	2.90	5.14	17.48	16.98	4.99
				WEC2	1.01	3.46	0.23	3.00				
				WEC3	1.00	3.44	0.23	3.00				
				WEC4	1.01	3.46	0.23	3.00				
				WEC5	1.06	3.56	0.23	2.90				
		5D	5	WEC1	1.03	3.45	0.24	3.00	5.30	17.56	16.46	4.96
				WEC2	1.07	3.53	0.24	3.00				
				WEC3	1.09	3.60	0.24	2.90				
				WEC4	1.07	3.53	0.24	3.00				
				WEC5	1.03	3.45	0.24	3.00				
3	1	-	6	WEC1	2.00	5.82	0.88	8.90	2.00	5.82	18.57	6.37
	3	2D	7	WEC1	2.21	6.18	0.92	8.80	6.62	18.32	16.83	6.08
				WEC2	2.19	5.96	0.96	8.90				
				WEC3	2.21	6.18	0.92	8.80				
		5D	8	WEC1	2.00	5.94	0.86	8.90	6.11	18.24	18.23	6.10
				WEC2	2.11	6.36	0.84	8.80				
				WEC3	2.00	5.94	0.86	8.90				
	5	2D	9	WEC1	2.26	6.31	0.92	8.80	11.81	32.25	15.71	5.75
				WEC2	2.40	6.48	0.96	8.80				
				WEC3	2.49	6.66	0.97	8.80				
				WEC4	2.40	6.48	0.96	8.80				
				WEC5	2.26	6.31	0.92	8.80				
		5D	10	WEC1	2.05	6.01	0.87	8.80	10.30	30.61	18.02	6.06
				WEC2	2.10	6.27	0.84	8.80				
				WEC3	2.00	6.05	0.84	8.90				
				WEC4	2.10	6.27	0.84	8.80				
				WEC5	2.05	6.01	0.87	8.80				
4	1	-	11	WEC1	4.00	9.02	2.45	17.50	4.00	9.02	15.70	6.96
	3	2D	12	WEC1	4.72	10.23	2.57	17.40	14.57	30.75	12.94	6.13
				WEC2	5.13	10.29	2.87	17.50				
				WEC3	4.72	10.23	2.57	17.40				
		5D	13	WEC1	3.94	9.21	2.34	17.50	11.94	28.07	15.79	6.72
				WEC2	4.05	9.64	2.27	17.40				
				WEC3	3.94	9.21	2.34	17.50				
	5	2D	14	WEC1	4.46	9.67	2.60	17.60	25.13	52.55	12.50	5.98
				WEC2	5.31	10.78	2.82	17.40				
				WEC3	5.60	11.67	2.70	17.20				
				WEC4	5.31	10.78	2.82	17.40				
				WEC5	4.46	9.67	2.60	17.60				
		5D	15	WEC1	3.98	9.25	2.35	17.50	19.74	47.00	15.92	6.68
				WEC2	3.95	9.54	2.24	17.50				
				WEC3	3.86	9.42	2.21	17.50				
				WEC4	3.95	9.54	2.24	17.50				
				WEC5	3.98	9.25	2.35	17.50				

Table 2. Extracted power and cost indicator for WECs placed in front of a vertical seawall, calculated for the optimal PTO damping at a natural frequency and the PTO damping for the maximum power (denoted as "optimum" and "maximum" respectively).

D (m)	N	L	Case		$\overline{P}_{irr}$ (kW)		b_{PTO} (kNs/m)		P_{Total} (kW)		Cost Indicator (m^3/kW)	
					Opt	Max	Opt	Max	Opt	Max	Opt	Max
2	1	-	1	WEC1	4.50	12.21	0.31	3.00	4.50	12.21	3.87	1.43
	3	2D	2	WEC1	4.91	12.66	0.33	3.00	14.48	37.54	3.61	1.39
				WEC2	4.67	12.20	0.32	3.00				
				WEC3	4.91	12.66	0.33	3.00				
		5D	3	WEC1	4.86	12.94	0.31	2.90	14.97	39.26	3.49	1.33
				WEC2	5.25	13.38	0.33	2.90				
				WEC3	4.86	12.94	0.31	2.90				
	5	2D	4	WEC1	5.31	13.75	0.33	2.90	26.82	67.64	3.25	1.29
				WEC2	5.36	13.40	0.34	3.00				
				WEC3	5.48	13.34	0.35	3.00				
				WEC4	5.36	13.40	0.34	3.00				
				WEC5	5.31	13.75	0.33	2.90				
		5D	5	WEC1	4.73	12.58	0.32	3.00	24.95	65.27	3.49	1.34
				WEC2	5.13	13.20	0.33	3.00				
				WEC3	5.24	13.71	0.32	2.90				
				WEC4	5.13	13.20	0.33	3.00				
				WEC5	4.73	12.58	0.32	3.00				
3	1	-	6	WEC1	9.46	18.78	1.46	8.90	9.46	18.78	3.92	1.98
	3	2D	7	WEC1	12.20	22.26	1.64	8.70	37.01	66.44	3.01	1.68
				WEC2	12.60	21.93	1.78	8.80				
				WEC3	12.20	22.26	1.64	8.70				
		5D	8	WEC1	9.74	19.39	1.46	8.90	30.18	60.61	3.69	1.84
				WEC2	10.69	21.84	1.39	8.80				
				WEC3	9.74	19.39	1.46	8.90				
	5	2D	9	WEC1	12.26	22.81	1.59	8.70	70.22	124.23	2.64	1.49
				WEC2	14.64	25.61	1.74	8.60				
				WEC3	16.42	27.39	1.86	8.60				
				WEC4	14.64	25.61	1.74	8.60				
				WEC5	12.26	22.81	1.59	8.70				
		5D	10	WEC1	10.20	19.86	1.50	8.80	51.07	102.11	3.63	1.82
				WEC2	10.55	21.29	1.42	8.70				
				WEC3	9.56	19.82	1.39	9.00				
				WEC4	10.55	21.29	1.42	8.70				
				WEC5	10.20	19.86	1.50	8.80				
4	1	-	11	WEC1	15.75	24.79	4.19	17.50	15.75	24.79	3.99	2.53
	3	2D	12	WEC1	21.93	32.50	4.54	17.00	72.23	101.43	2.61	1.86
				WEC2	28.37	36.44	5.85	16.50				
				WEC3	21.93	32.50	4.54	17.00				
		5D	13	WEC1	14.84	24.93	3.79	17.60	44.62	76.32	4.22	2.47
				WEC2	14.93	26.46	3.50	17.70				
				WEC3	14.84	24.93	3.79	17.60				
	5	2D	14	WEC1	19.27	28.62	4.65	17.60	124.35	173.59	2.53	1.81
				WEC2	28.16	37.22	5.59	16.80				
				WEC3	29.49	41.90	4.84	16.70				
				WEC4	28.16	37.22	5.59	16.80				
				WEC5	19.27	28.62	4.65	17.60				
		5D	15	WEC1	15.25	25.16	3.88	17.60	72.55	127.30	4.33	2.47
				WEC2	14.28	25.92	3.39	17.80				
				WEC3	13.49	25.15	3.26	17.80				
				WEC4	14.28	25.92	3.39	17.80				
				WEC5	15.25	25.16	3.88	17.60				

These results are further plotted below for a detailed analysis. In Figure 9, the total power output of various configurations of an array is assessed both for WECs without a vertical seawall and those with a vertical seawall. WECs situated in front of the seawall exhibited greater power extraction by the increase of WECs' heave motion due to the formation of standing waves. Also, the extracted power drastically increased with the diameter as the larger WEC possesses the potential to accommodate larger PTO damping, enabling higher power absorption.

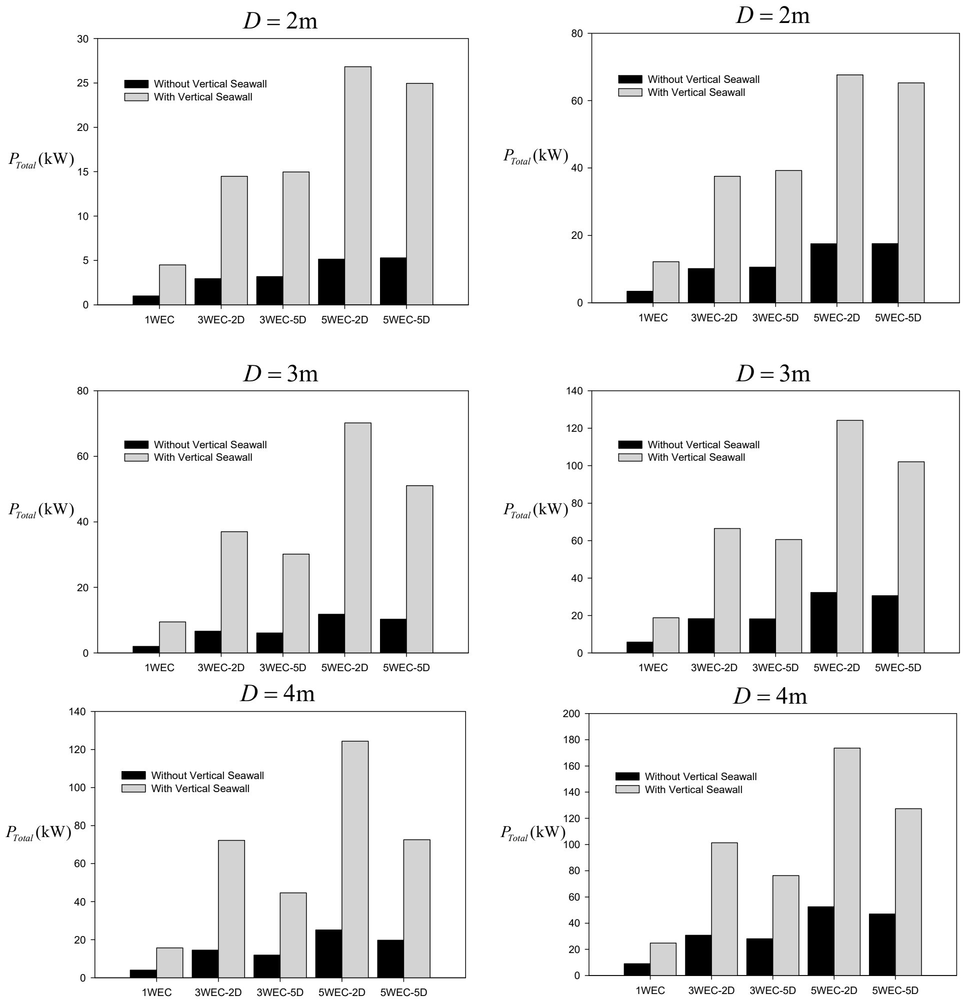

(**a**) optimum (**b**) maximum

Figure 9. Comparison of total power for each configuration of an array of WECs placed in the open sea and in front of a vertical seawall for different diameters of the WEC.

To understand how the number of WEC in an array and the distance between WECs affects the power absorption of each WEC, the "optimum" extracted power of each WEC in an array configuration of single, three, and five WECs with a distance of 2D and 5D between WECs is compared in Figure 10.

The heave motion of the inside-positioned WECs in an array influenced the motion of adjacent WECs. However, the outside-positioned WECs facing the open sea on one side were only affected by the neighboring WEC on the other side. The WECs positioned at the symmetrical placement in an array had the same performance. Therefore, the power extracted from the centered WEC and the outmost WEC in an array were compared, as these serve as representative WECs for the analysis. For the single WEC, the outmost WEC and centered WEC are the same.

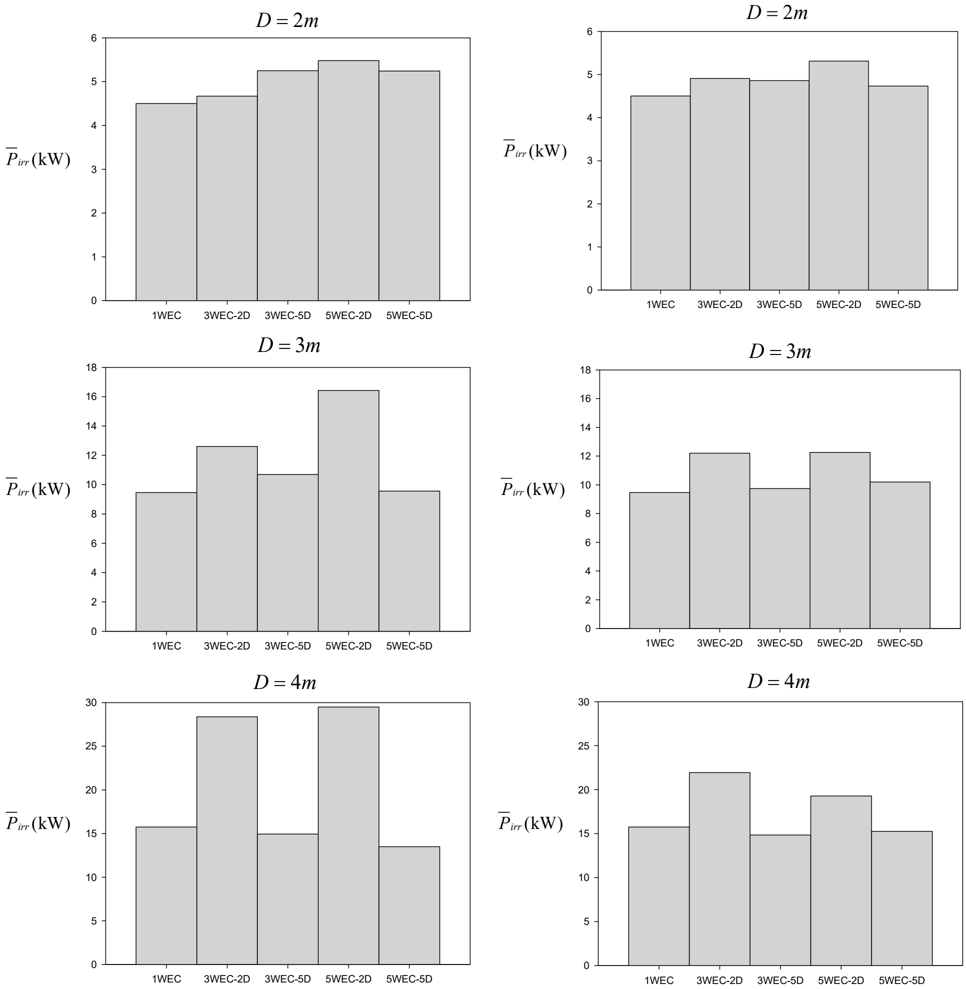

(**a**) Centered WEC in an array (**b**) Outmost WEC in an array

Figure 10. Comparison of wave power extracted from each WEC in the configuration of a single WEC and multiple WECs placed in front of the vertical seawall calculated for the "optimum" PTO.

It is noticed from Figure 10 that when compared to a single WEC, configurations with three and five WECs exhibited an increase in power of each WEC, especially five WECs. This enhancement was a result of the interaction between neighboring WECs due to the presence of trapped waves between them. The trapped waves between WECs, coupled with the standing waves resulting from the reflection of incident waves against the vertical seawall, significantly intensified wave fields and consequently amplified the heave motion of each WEC. Thus, the centered WEC showed higher power absorption because of higher interactions of adjacent WECs than the outmost WEC which is open to sea on one side. Likewise, the intermediate WECs (②, ④) in an array of 5 WECs showed increased power extraction. Therefore, an increase in the number of WECs results in increased interactions among them, contributing to the enhanced power output of each WEC. However, the extracted power would also depend on the distance between WECs, which might constructively or destructively affect the performance. Among all cases of multiple WECs, a separation distance of 2D between WECs exhibited greater power enhancement compared to 5D, except for the 2 m diameter with an array of 3 WECs, where only a marginal difference was observed. Notably, the WECs with larger diameters demonstrated a substantial increase in the power extraction for the closer distance. This power enhancement could be attributed to higher interactions among WECs while keeping a closer distance between them than keeping them farther apart. Hence, these individual power enhancements of each WEC within an array collectively contribute to a higher overall power output. The same observations held when employing the "maximum" power calculation method. Therefore, an increased number of WECs arranged in an array with shorter distances between them would be the optimal configuration for maximizing power extraction.

3.5. Ranking of a Cost-Effective Array of WECs

The cost-effectiveness of various configurations of an array of WECs is assessed based on a cost indicator, which reflects the cost associated with extracting unit power. In Figures 11 and 12, the cost-effective configurations are prioritized according to the cost indicator, with the most favorable scenarios placed at the top of the plots. The WECs placed in front of a vertical seawall have substantially reduced the cost indicator with greater power extraction. This occurred because the vertical seawall increases the heave motion of WEC due to the formation of standing waves, resulting in increased power output for the equivalent submerged volume.

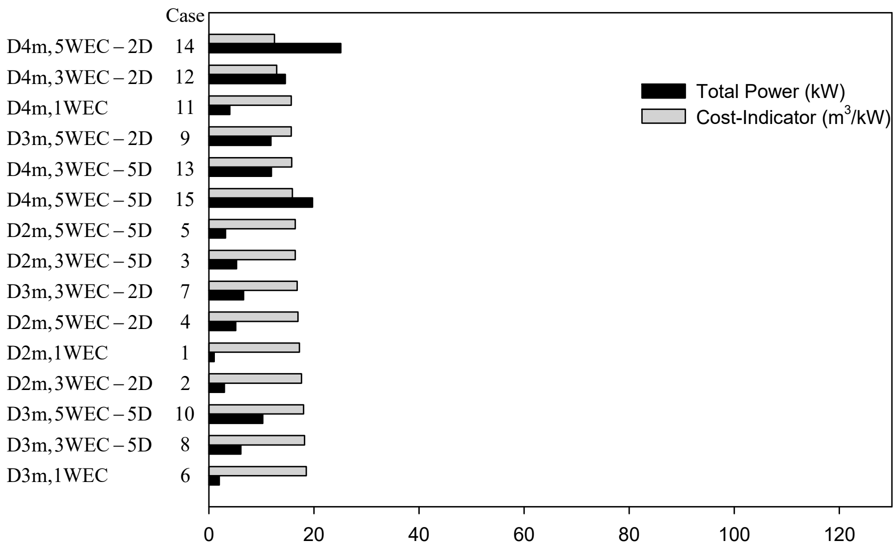

(**a**) Without Vertical Seawall

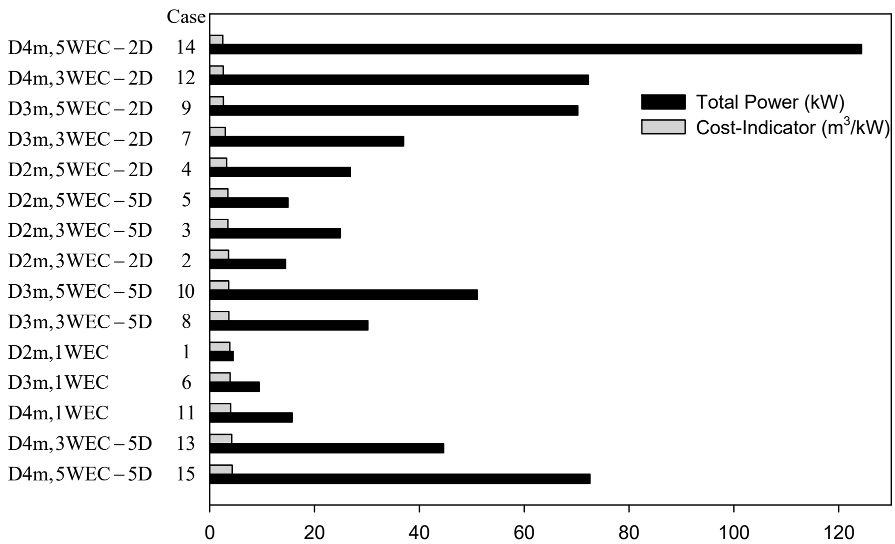

(**b**) With Vertical Seawall

Figure 11. Ranking of the cost-effectiveness of configurations of WECs based on the "optimum" power calculation method.

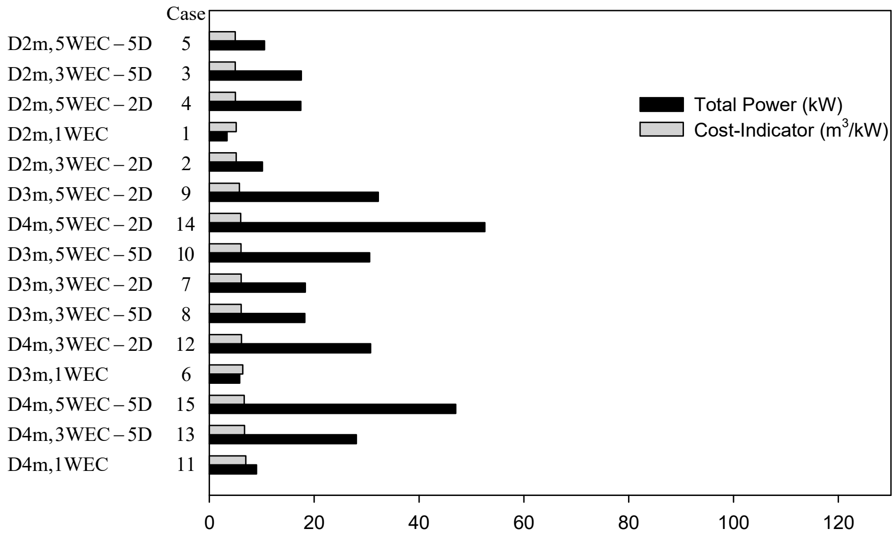

(**a**) Without a vertical seawall

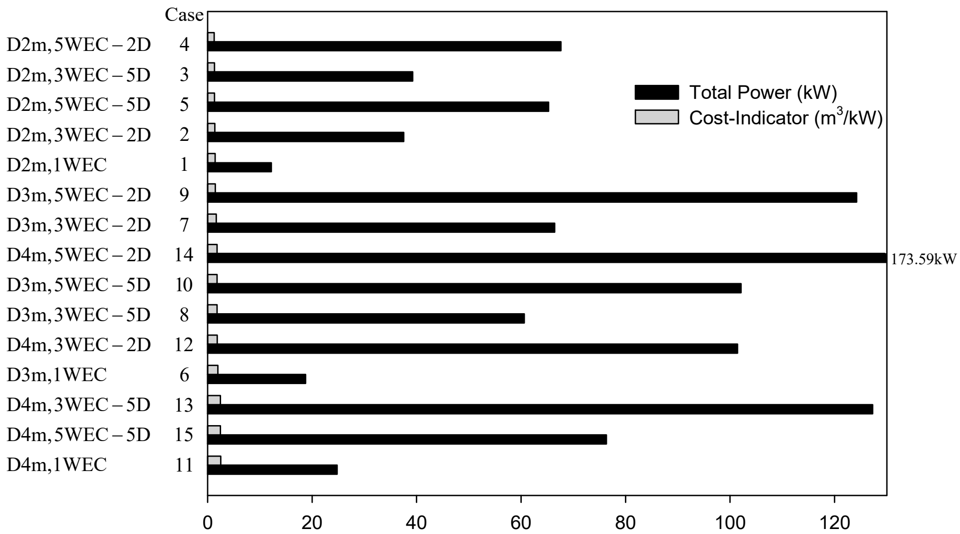

(**b**) With a vertical seawall

Figure 12. Ranking of the cost-effectiveness of configurations of WECs based on the "maximum" power calculation method.

In Figure 11, the trend indicates that the WECs with the sequence of larger-to-smaller diameter, when combined with an increase in the number of WECs in an array and positioned closer together, tended to achieve superior rankings in cost-effectiveness under the "optimum" power calculation method. In contrast, when employing the "maximum" calculation method, the WECs with the decrease of the diameter of WECs tended to attain a superior ranking as shown in Figure 12. When utilizing the "optimum" calculation method, larger diameters tended to exhibit effective PTO damping for maximizing power extraction for an equivalent submerged volume. Conversely, the "maximum" calculation method provided an opportunity for smaller diameters to accommodate efficient damping from a range of PTO damping which yields higher power output for an equivalent submerged volume.

4. Conclusions

An assessment was conducted to determine the cost-effective configuration of an array of WECs positioned in front of a vertical seawall in irregular waves. It involved a parametric study of varying diameters, number of WECs, and distances between the WECs. The WEC oscillates vertically in heave motion while utilizing a linear PTO damping system to harness wave power. The hydrodynamic parameters were numerically obtained using WAMIT with the method of image to incorporate the influence of the vertical seawall. These numerical calculations were validated against previously published analytical results. The viscous damping was obtained from a CFD simulation of the free decay test, which was validated beforehand against the experimental measurement for the cylinder model in a 2D wave tank. The power calculations were performed using both the optimal PTO damping at a natural frequency and the PTO damping that result in maximum power output. The cost-effectiveness was evaluated using a cost indicator, represented as the ratio of the total submerged volume of WECs to the overall power captured which reflects the production cost associated with extracting a unit power.

Based on the parametric analysis, the WECs placed in front of the vertical seawall achieve greater power extraction compared to the WECs placed in the open sea. The formation of standing waves due to total reflection by vertical seawall increases the heave motion of WECs, leading to higher power extraction. When compared to a single WEC, an increase in the number of WECs in an array shows higher power absorption due to interactions among WECs caused by trapped waves between them. The cost-effectiveness of WECs increases when the WECs are placed in front of the seawall, with a larger number of WECs in an array while keeping a shorter distance between them. The larger diameter of WECs excels in cost-effectiveness rankings when considering the optimal PTO damping at a natural frequency, whereas the smaller diameter of WECs exhibits superior performance with the PTO damping for maximum power extraction. These differences are attributed to the methods employed in implementing effective PTO damping, which enables higher power output for an equivalent submerged volume of WEC.

These findings demonstrate that achieving economically efficient wave power extraction is possible by installing multiple WECs in front of a reflecting seawall, even in nearshore shallow water regions. The shorter distance between WECs and the larger number of WECs in an array enables the production of more power. In addition, the nearshore installation of WECs also allows cost-effective power transmission connectivity to the onshore grid and the cost associated with maintenance compared to the offshore installation. Nevertheless, the challenges associated with nearshore installation encompass securing suitable space for WEC installation, implementing PTO systems, and establishing grid connectivity, particularly in densely developed coastal areas, could pose significant hurdles that must be addressed. These multiple WECs can also be installed in front of the offshore wind power platform that has a reflective wall similar to the seawall. This hybrid power system utilizing wind and wave power simultaneously could potentially offer cost-effectiveness by sharing the supported structure, power grid, and connectivity.

Author Contributions: Conceptualization, S.K.N.; Methodology, S.K.N.; software, S.K.N.; validation, S.K.N.; investigation, S.K.N.; writing—original draft preparation, S.K.N.; writing—review and editing, I.H.C.; supervision, I.H.C.; funding acquisition, I.H.C. All authors have read and agreed to the published version of the manuscript.

Funding: This research was supported by the Basic Science Research Program through the National Research Foundation of Korea (NRF) funded by the Ministry of Education (NRF-2022R1I1A3066608).

Data Availability Statement: Data is contained within the article.

Conflicts of Interest: The authors declare no conflicts of interest.

References

1. Hannah Ritchie and Max Roser, Emissions by Sector. Available online: https://ourworldindata.org/emissions-by-sector (accessed on 16 November 2023).
2. IEA. *World Energy Outlook 2022*; IEA: Paris, France, 2022.
3. McCormick, M.E. *Ocean Wave Energy Conversion*; Dover Publication Inc.: New York, NY, USA, 2007; Chapter 1.
4. Astariz, S.; Iglesias, G. The economics of wave energy: A review. *Renew. Sustain. Energy Rev.* **2015**, *45*, 397–408. [CrossRef]

5. Lyu, J.; Abdelkhalik, O.; Gauchia, L. Optimization of dimensions and layout of an array of wave energy converters. *Ocean Eng.* **2019**, *192*, 106543. [CrossRef]
6. Zhong, Q.; Yeung, R.W. On optimal energy-extraction performance of arrays of wave-energy converters, with full consideration of wave and multi-body interactions. *Ocean Eng.* **2022**, *250*, 110863. [CrossRef]
7. Guo, B.; Ringwood, J.V. Geometric optimisation of wave energy conversion devices: A survey. *Appl. Energy* **2021**, *297*, 117100. [CrossRef]
8. Garcia-Teruel, A.; Forehand, D.I.M. A review of geometry optimisation of wave energy converters. *Renew. Sustain. Energy Rev.* **2021**, *139*, 110593. [CrossRef]
9. Rodríguez, C.A.; Rosa-Santos, P.; Taveira-Pinto, F. Hydrodynamic optimization of the geometry of a sloped-motion wave energy converter. *Ocean Eng.* **2020**, *199*, 107046. [CrossRef]
10. Zhang, X.; Li, B.; Hu, Z.; Deng, J.; Xiao, P.; Chen, M. Research on Size Optimization ofWave Energy Converters Based on a Floating Wind-Wave Combined Power Generation Platform. *Energies* **2022**, *15*, 8681. [CrossRef]
11. Sun, P.; Hu, S.; He, H.; Zheng, S.; Chen, H.; Yang, S.; Ji, Z. Structural optimization on the oscillating-array-buoys for energy-capturing enhancement of a novel floating wave energy converter system. *Energy Convers. Manag.* **2021**, *228*, 113693. [CrossRef]
12. Shadmani, A.; Nikoo, M.R.; Al-Raoush, R.I.; Alamdari, N.; Gandomi, A.H. The Optimal Configuration of Wave Energy Conversions Respective to the Nearshore Wave Energy Potential. *Energies* **2022**, *15*, 7734. [CrossRef]
13. Sheng, W.; Lewis, A. Power takeoff optimization for maximizing energy conversion of wave-activated bodies. *IEEE J. Ocean. Eng.* **2016**, *41*, 529–540. [CrossRef]
14. Loukogeorgaki, E.; Chatjigeorgiou, I.K. Hydrodynamic performance of an array of truncated cylinders in front of a vertical wall. *Ocean Eng.* **2019**, *189*, 106407. [CrossRef]
15. Zhao, X.L.; Ning, D.Z.; Liang, D.F. Experimental investigation on hydrodynamic performance of a breakwater-integrated WEC system. *Ocean Eng.* **2019**, *171*, 25–32. [CrossRef]
16. Zhang, C.; Ning, D. Hydrodynamic study of a novel breakwater with parabolic openings for wave energy harvest. *Ocean Eng.* **2019**, *182*, 540–551. [CrossRef]
17. Konispoliatis, D.N.; Mavrakos, S.A.; Katsaounis, G.M. Theoretical evaluation of the hydrodynamic characteristics of arrays of vertical axisymmetric floaters of arbitrary shape in front of a vertical breakwater. *J. Mar. Sci. Eng.* **2020**, *8*, 62. [CrossRef]
18. Konispoliatis, D.N.; Mavrakos, S.A. Wave power absorption by arrays of wave energy converters in front of a vertical breakwater: A theoretical study. *Energies* **2020**, *13*, 1985. [CrossRef]
19. Konispoliatis, D.N.; Mavrakos, S.A. Hydrodynamic efficiency of a wave energy converter in front of an orthogonal breakwater. *J. Mar. Sci. Eng.* **2021**, *9*, 94. [CrossRef]
20. Kara, F. Hydrodynamic performances of wave energy converter arrays in front of a vertical wall. *Ocean Eng.* **2021**, *235*, 109459. [CrossRef]
21. Kara, F. Effects of a vertical wall on wave power absorption with wave energy converters arrays. *Renew. Energy* **2022**, *196*, 812–823. [CrossRef]
22. Sirigu, S.A.; Foglietta, L.; Giorgi, G.; Bonfanti, M.; Cervelli, G.; Bracco, G.; Mattiazzo, G. Techno-Economic optimisation for a wave energy converter via genetic algorithm. *J. Mar. Sci. Eng.* **2020**, *8*, 482. [CrossRef]
23. Tan, J.; Polinder, H.; Laguna, A.J.; Wellens, P.; Miedema, S.A. The influence of sizing of wave energy converters on the techno-economic performance. *J. Mar. Sci. Eng.* **2021**, *9*, 52. [CrossRef]
24. Têtu, A.; Fernandez Chozas, J. A proposed guidance for the economic assessment of wave energy converters at early development stages. *Energies* **2021**, *14*, 4699. [CrossRef]
25. Giglio, E.; Petracca, E.; Paduano, B.; Moscoloni, C.; Giorgi, G.; Sirigu, S.A. Estimating the Cost of Wave Energy Converters at an Early Design Stage: A Bottom-Up Approach. *Sustainability* **2023**, *15*, 6756. [CrossRef]
26. He, Z.; Ning, D.; Gou, Y.; Zhou, Z. Wave energy converter optimization based on differential evolution algorithm. *Energy* **2022**, *246*, 123433. [CrossRef]
27. Babarit, A. Impact of long separating distances on the energy production of two interacting wave energy converters. *Ocean Eng.* **2010**, *37*, 718–729. [CrossRef]
28. Cho, I.H.; Kim, M.H. Hydrodynamic performance evaluation of a wave energy converter with two concentric vertical cylinders by analytic solutions and model tests. *Ocean Eng.* **2017**, *130*, 498–509. [CrossRef]
29. Zhou, B.Z.; Hu, J.J.; Sun, K.; Liu, Y.; Collu, M. Motion response and energy conversion performance of a heaving point absorber wave energy converter. *Front. Energy Res.* **2020**, *8*, 553295. [CrossRef]
30. Natarajan, S.K.; Cho, I. New Strategy on Power Absorption of a Concentric Two-Body Wave Energy Converter. *Energies* **2023**, *16*, 3791. [CrossRef]
31. Goda, Y. Statistical variability of sea state parameters as a function of a wave spectrum. *Coast. Eng. Jpn.* **1988**, *31*, 39–52. [CrossRef]
32. Bhattacharyya, R. *Dynamics of Marine Vehicles*; John Wiley & Sons Incorporated: Hoboken, NJ, USA, 1978; Chapter 6.
33. Newman, J.N. *Marine Hydrodynamics*, 40th Anniversary ed.; The MIT Press: London, UK, 2018; Chapter 6.